Structural characterization of the EmrAB-TolC efflux complex from E. coli

Narek Yousefian, Alina Ornik-Cha, Sylvie Poussard, Marion Decossas, Melanie Berbon, Laetitia Daury, Jean-Christophe Taveau, Jean-William Dupuy, Selena Đorđević-Marquardt, Olivier Lambert, et al.

Structural characterization of the EmrAB-TolC efflux complex from *E. coli*

Narek Yousefian[1,3], Alina Ornik-Cha[3], Sylvie Poussard[1#], Marion Decossas[1#], Melanie Berbon[1], Laetitia Daury[1], Jean-Christophe Taveau[1], Jean-William Dupuy[2], Selena Đorđević[3], Olivier Lambert[1 *] and Klaas M. Pos[3] *

[1]Univ. Bordeaux, CBMN UMR 5248, Bordeaux INP, F-33600 Pessac, France.
[2]Univ. Bordeaux, Plateforme Protéome, 33000, Bordeaux, France,
[3] Institute of Biochemistry, Goethe-University Frankfurt, Max-von-Laue-Str. 9, D-60438 Frankfurt am Main, Germany

# contributed equally
* Correspondence to Klaas M. Pos (pos@em.uni-frankfurt.de) or Olivier Lambert (olivier.lambert@u-bordeaux.fr)

Abstract

Gram-negative bacteria export a large variety of antimicrobial compounds by forming two-membrane spanning tripartite multidrug efflux systems composed of an inner membrane transporter, an outer membrane channel and a periplasmic adaptor protein. Here we present the co-expression, purification and first electron microscopy insights of the *Escherichia coli* EmrAB–TolC tripartite Major Facilitator Superfamily (MSF) efflux system as a whole complex stabilized by Amphipol polymer. The structure reveals a 33 nm long complex delineated by the Amphipol belt at both extremities. Comparison of projection structures of EmrAB-TolC and AcrAB-TolC indicates that the outer membrane protein TolC linked to the periplasmic adaptor EmrA protein form an extended periplasmic canal. The overall length of EmrAB-TolC complex is similar to that of AcrAB-TolC with a probable tip-to-tip interaction between EmrA and TolC unveiling how the adaptor protein connects TolC and EmrB embedded in the inner membrane.

Introduction

Tripartite efflux systems contribute substantially to the intrinsic or acquired antibiotic resistance of numerous Gram negative bacteria [1–3]. Such complexes (RND, ABC and MFS-type) are composed of an inner membrane drug specificity and energy transduction component, an outer membrane exit duct and a periplasmic adaptor protein connecting both transmembrane partners [4,5]. A continuous effort has led to increasing information about the structural organization of these complexes from different families (*e.g.* RND and ABC) [4,6–9][45]. The most functionally and structurally studied systems are the RND-based AcrAB-TolC and MexAB-OprM efflux pumps and recently the structure ABC-type MacAB-TolC tripartite system has been determined. Despite these successes, little is known about the MFS-based tripartite efflux systems, such as EmrAB-TolC. The *emrAB* operon was first identified 28 years ago [10] as conferring intrinsic resistance of *E. coli* to carbonyl - cyanide *m*-

chlorophenylhydrazone (CCCP) and nalidixic acid [10,11]. Its overexpression, due to either induction or by a repressor mutation, causes increased resistance to nalidixic acid, thiolactomycin, nitroxoline, hydrophobic proton uncouplers [10–13]. The inner membrane drug proton antiporter EmrB has 14 putative transmembrane helices (TMS), but structural and functional analysis has been sparse. Structures of other homologous MFS-type 12 TMS drug transporters, like MdfA and EmrD, as well as the 14 TMS peptide transporter $PepT_{So}$ are known [14–17]. Whereas for the RND-type transporters it is postulated that these systems sequester their substrates from the periplasmic side of the Gram-negative inner membrane, it is suggested that the MFS-type transporter EmrB recognizes its substrates from the cytoplasm or the inner leaflet of the inner membrane. Substrates are subsequently released on the periplasmic side inside the channel-like EmrA multimeric adaptor component, connected to the well-known TolC outer membrane channel, leading the toxic compounds across the outer membrane. The structure of the adaptor protein EmrA from *Aquifex aeolicus* was solved by X-ray crystallography and revealed three distinct domains (β-barrel, lipoyl and α-helical coiled-coil domains), akin to the domain architecture in the hexameric MexA and AcrA [4] [18]. However, the stoichiometry of EmrA within the entire system is still unclear, even if the adaptor protein was found to form dimers and trimers *in vitro* [19], and previous negative staining EM analyses suggest the formation of a physiological EmrAB complex being a ‘dimer of dimers’ [20]. The trimeric exit duct TolC is divided into the β-barrel outer membrane (OM) channel and a periplasmic α-helical tunnel domain [21] that interact with RND and ABC adapter molecules in a tip to tip manner [4].

The study presented here describes a strategy to overexpress and isolate the entire tripartite EmrAB-TolC assembly directly from cells for subsequent structural analysis. The three components were co-expressed and extracted from the inner and outer membranes as an intact complex using mild solubilization conditions. Single particle EM analysis revealed the

overall architecture of the EmrAB-TolC efflux complex from *E. coli* as well as the relative arrangement of its components.

Methods

Construction of plasmids for the overexpression of the EmrAB-TolC complex

For the Fragment eXchange (FX) cloning method [22], *E. coli* MC1061[23], DB3.1 [24], and DH5α [25] were used as cloning hosts. The p7XC3RH and pRSFDMG vectors used in this work were derivatives of the p7XC3GH [22] and pRSFDuet [26] vectors, respectively. The *emrA*, *emrB* and *tolC* genes were amplified by PCR from the genomic DNA of *E. coli* BL21 [27] strain (Supplementary Table1). Each insert was cloned into the SapI site of the FX initial cloning vector (pINITIAL) [22] to obtain pINIT_*emrA*, pINIT_*emrB*, and pINIT_*tolC*. The inserts were sequenced for verification (Microsynth). The FX-expression vector p7XC3RH_*emrB* was constructed by FX-cloning the *emrB* gene from pINIT_*emrB* into the SapI site of p7XC3RH (Figure S1A) so that it encodes EmrB with a C-terminal mRFP1-His tag fusion protein.

TolC was amplified by PCR from pINIT_*tolC* with primers TolCNdeI_F: 5'-GGGAATTCCATATGAAGAAATTGCTCCCCATTCT-3' and TolCPacI_R: 5'-CCTTAATTAAGTTACGGAAAGGGTTATGAC-3' to facilitate cloning into the NdeI/PacI site of the FX-compatible expression vector pRSFDMG to generate pRSFDMG_*tolC*. The insert was sequenced for verification (Microsynth). The insert encodes TolC including a C-terminal Strep-tagII. The FX-compatible expression vector pRSFDMG_*emrA_tolC* (Figure S1B) was generated by subcloning *emrA* from the initial FX-cloning vector pINIT_*emrA* into the SapI site of the vector pRSFDMG_*tolC*. This plasmid encodes besides C-terminal Strep-tagII fused TolC, EmrA with a C-terminally fused superfolder-GFP variant (sfGFP) and c-Myc-tag.

EmrAB-TolC co-expression in 96-deepwell blocks

E. coli BL21(DE3) [28], C41(DE3)Δ*acrAB* [29], C43(DE3) [29], and BW25113(DE3)Δ*acrAB* [30] harbouring both p7XC3RH_*emrB* and pRSFDMG_*emrA_tolC* were cultivated in 2xYT medium supplemented with 50 μg/mL Kanamycin and 100 μg/mL Ampicillin at 37°C under vigorous aeration. Cultivation of each strain was started with a 1% inoculum of an overnight culture of each strain in LB containing antibiotics. Upon growth to OD_{600}≈0.6, cells were incubated for 20 min on ice before induction with ten different concentrations of IPTG [Isopropyl-β-D-thiogalactopyranoside] (0.1-1 mM). Growth was subsequently continued overnight at 25°C. After centrifugation, cell pellets were suspended in 200 μL phosphate buffered saline pH 7.4. Red and green fluorescence signals (excitation and emission wavelengths at 576 nm and 610 nm respectively for red signal and 485 nm and 535 nm respectively for green signal) were measured in a microplate reader (TECAN reader infinite 200, Tecan Trading AG, Switzerland) and normalized with OD_{600} since *E. coli* C41(DE3) and *E. coli* C43(DE3) continue to grow after IPTG induction [29] due to mutations in the lacUV5 promotor region [31].

EmrAB-TolC co-production and co-purification.

The EmrAB-TolC complex was overproduced in *E. coli* C41(DE3)Δ*acrAB* cells in 2 L of 2xYT medium in 5L baffled flask at 37°C under vigorous agitation. At OD_{600} = 0.6, the culture was cooled down in an ice/water bath, and IPTG was added (0.5 mM final concentration) before further growth at 25°C overnight whilst shaking. Cells were harvested by centrifugation at 8,000 *g* for 20 minutes and resuspended in 2 ml per g cells in ice-cold buffer A (50 mM Tris/Cl, pH 7.5, 400 mM NaCl, 2 mM EDTA, 10 mM $MgCl_2$, 2 mM $CaCl_2$, 0.2 mM diisopropyl fluorophosphate, and 30 U/mL DNase I). Cells were gently disrupted

with the addition of 1 mg/mL lysozyme and shaken for 30 min at 37°C. After a centrifugation step at 25,000 g for 30 minutes, the pellet was resuspended in ice-cold buffer B (50 mM Tris/Cl, pH 7.5, 400 mM NaCl, and 210 U/mL DNaseI). Membrane proteins and complexes were solubilized with the addition of 2% final concentration of *n*-Dodecyl β-D-maltoside (DDM) for 2 h at 4°C. The insoluble fraction was removed by centrifugation for 60 minutes at 125,000 *g*. The supernatant was supplemented with 20 mM (final concentration) imidazole, filtered through a 0.22 µm filter (Sartorius, Germany) and subjected to Ni^{2+}-NTA chromatography (GE Healthcare, USA). The column (containing 5 mL bed volume of Ni-NTA resin) was pre-equilibrated with buffer C (50 mM Tris/Cl, pH 7.5, 150 mM NaCl, 0.025% DDM) supplemented with 20 mM (final concentration) imidazole before 30 mL of supernatant was applied to the column. Subsequently, the column was washed with 2 column bed volumes buffer C containing 20 mM and 50 mM imidazole respectively. Elution of the EmrAB-TolC complex was in buffer C containing 300 mM imidazole (50 mL). The 50 ml eluate was concentrated to 500 µl final volume with a 300 kDa cut-off concentrator (Sartorius, Germany) and subjected to size-exclusion chromatography (Superose 6 10/300 column, GE Healthcare, USA) in buffer C. Fractions 22-26 containing the EmrAB-TolC complex were pooled and concentrated to 1 mg/mL as described above. Amphipol A8-35 (Apol) (Anatrace, USA) at 10 mg/mL was mixed with the protein solution at a 4:1 Apol to protein mass ratio for 2 h at 4°C. Detergent was removed by the addition of SM2 Bio-beads (60 mg/mL; Bio-Rad, USA) with gentle shaking for 3h at 4°C. After centrifugation, the mixture was subjected to size-exclusion chromatography (Superose 6 3.2/300, GE Healthcare, USA) equilibrated with buffer D (50 mM Tris/Cl, pH 7.5, 150 mM NaCl, 0.01 % NaN_3). Fractions containing the complex were further analyzed by SDS-PAGE and silver staining (GE Healthcare).

EmrB expression and purification

E. coli strain C41(DE3)Δ*acrAB* transformed with p7XC3RH_*emrB* vector was cultivated as described for EmrAB-TolC production. Cells harvested by centrifugation were resuspended in buffer A during 30 min at 4°C and were disrupted by three passage through a French pressure cell (20,000 psi). After a centrifugation step (10,000 g) to eliminate cell debris and unbroken cells (4°C, 30 min), the supernatant was centrifuged at 100,000 g for 2h at 4°C. The resulting pellet containing the membranes resuspended in Tris buffer (50 mM Tris/Cl, pH 8, 200 mM NaCl) containing 2% DDM and cocktail inhibitor tablet (Roche) was mildly shaken for 1 h at 4 °C. The membrane lysate was diluted 5 times in Tris buffer without DDM and centrifuged at 100,000 *g* for 1h at 4°C. The resulting supernatant was used to purify EmrB-mRFP1 using the same protocol as described above for the EmrAB-TolC complex except that EmrB-mRFP1 was eluted from the Ni^{2+}-NTA column with 400 mM imidazole after a washing step with 80 mM imidazole buffer containing 5 mM ATP to remove heat-shock protein (Hsp) contamination. The eluate was dialyzed overnight in Tris buffer containing 0.025% DDM without imidazole and concentrated to 1 mg/mL using a 10 kDa cut-off concentrator (Sartorius).

EmrB-mRFP1 (1.5 mg) was incubated overnight at 4°C with HIS10-HRV 3C (rhinovirus 3C) protease (15 µg, Pierce). The incubation mixture was subsequently subjected to Ni^{2+}-NTA chromatography. EmrB was recovered in the flow-through using one column bed volume Tris buffer, while the His-tagged HRV 3C protease and His-tagged mRFP1 were retained on the column. The concentrated EmrB (0.5 mg/mL) in Tris buffer containing 0.025% DDM was reconstituted in Apol as described above. Fractions containing EmrB were further analyzed by SDS-PAGE and Coomassie staining.

Proteomic analysis

Protein digestion by chymotrypsin was performed as previously described [32]. NanoLC-MS/MS analysis were performed using an Ultimate 3000 RSLC Nano-UPHLC system (Thermo Scientific, USA) coupled to a nanospray Orbitrap Fusion™ Lumos™ Tribrid™ Mass Spectrometer (ThermoFisher Scientific). Mascot, Sequest and Amanda algorithms through Proteome Discoverer 2.3 Software (ThermoFisher Scientific Inc.) were used for protein identification in batch mode by searching against a merge of protein databases: UniProt *Escherichia coli BL21_DE3* database (UP000002032, release 18/11/09, 31587 entries) and the sequence of the recombinant protein.

In-Gel Fluorescence, immunodetection.

Whole cell samples (cells from 1 mL culture at OD_{600} = 1) were suspended in 100 µL of 1X protein sample buffer (50 mM Tris/Cl, pH 6.8, 10 % (vol/vol) glycerol, 0.4% (vol/vol) 2-Mercaptoethanol, 1% (wt/vol) SDS, and 0.01% (wt/vol) bromophenol blue), heated at 37°C for 10 min and subsequently 15 µL of each sample per lane was subjected to 12% SDS-PAGE. In-gel mRFP1 or sfGFP fluorescence (excitation and emission wavelengths at 576 nm and 610 nm respectively for red signal and 485 nm and 535 nm respectively for green signal) was detected using a LAS-4000 imaging system (GE Healthcare, USA). Subsequently, gels were subjected to Western Blot analysis using a Roti-NC 0.2 µm nitrocellulose membrane (Carl Roth GmbH + Co. KG) for transfer of proteins during 30 min at 25 V in transfer buffer (25 mM Tris/Cl, 192 mM glycine, 20 % methanol, pH 8.3). The membrane was subsequently blocked overnight in 3% BSA TBST (20 mM Tris/Cl, 150 mM NaCl, 0.1 % Tween 20, pH 8) at 4°C. For the immunological detection of EmrB, an alkaline phosphatase conjugated antibody raised against a His_6-tag (Merck KGaA, Germany) was used. EmrA-myc was detected with a primary antibody raised against a c-Myc tag (Merck KGaA, Germany) combined with a secondary mouse anti-rabbit antibody alkaline phosphatase conjugate

(Merck KGaA, Germany). For the detection of TolC, a Strep-Tactin alkaline phosphatase conjugate (IBA Lifesciences, Germany) was used. To reveal the position of alkaline phosphatase on the blot, nitro blue tetrazolinum (NBT) and 5-bromo-4-chloro-3-indoyl phosphate (BCIP) were used.

Electron microscopy acquisition and analysis.

For EM grid preparations, sample suspensions were prepared as followed. Fractions A10 to A12 of EmrAB-TolC suspension were diluted three times in 50 mM Tris/Cl, pH 7.5, 150 mM NaCl, 0.01 % NaN_3 and Fractions B3 and B4 of EmrB suspension were diluted four times in the same buffer. Samples were applied to a glow-discharged carbon-coated copper 300 mesh grids and stained with 2% uranyl acetate (wt/vol) solution. Images were acquired on a Tecnai F20 electron microscope (ThermoFisher FEI) operated at 200kV using an Eagle 4k_4k camera (ThermoFisher FEI) and using serialEM software for automatic acquisition. Micrographs were collected with a nominal defocus range of −1.5 to -3 µm and a low dose of ~30 electrons/Å. Images were processed with EMAN2 software suite. For EmrAB-TolC EM analysis, a total of 518 particles was manually picked with a box size of 192×192 pixels (pixel size 2.94 Å) on the specimen level. For EmrB EM analysis, a total of 9732 particles was automatically picked with a box size of 165 x 165 pixels (pixel size 2.16 Å). As an independent analysis, a set of 4822 particles of Apol sample at 100 µg/mL was automatically picked with a box size of 118 x 118 pixels. For AcrAB-TolC EM analysis, a set of 900 particles was manually picked and analysed as described [33].

Results

Analysis of EmrA, EmrB and TolC expressions for several strains.

To determine the optimal conditions leading to a high level expression of both the inner membrane transporter EmrB and the adaptor protein EmrA, we used the fluorescent reporters mRFP1 and sfGFP as C-terminal fusions for assessing the expression levels of both proteins in the same cells (i.e. harbouring p7XC3RH_*emrB* and pRSFDMG_*emrA_tolC*, Figure S1) according to previously GFP-based reported methods [34–37]. EmrB-mRFP1 production as a result of IPTG induction could only be observed in *E. coli* C41(DE3) and *E. coli* C43(DE3), whereas IPTG induction did not result in increased mRFP1 signal in *E. coli* BL21(DE3) and BW25113(DE3). The red fluorescence signal strength was comparable for all IPTG concentrations tested (0.1 to 1mM) (Figure S2A). For EmrA-sGFP, the expression levels were significantly increased after IPTG induction in *E. coli* C41(DE3), C43(DE3) and BW25113(DE3) strains, but not for *E. coli* BL21(DE3) (Figure S2B). From this data, we considered *E. coli* C41(DE3) as the host with the highest EmrA and EmrB expression and therefore total cellular extracts of *E. coli* C41(DE3) (harbouring p7XC3RH_*emrB* and pRSFDMG_*emrA_tolC*) were used for EmrA-sGFP and EmrB-mRFP1 expression analysis via in gel fluorescence SDS-PAGE and Western blot analysis (Figure 1). Activity of the efflux pump could be shown after challenging *E. coli* BW25113(DE3) harbouring p7XC3RH_*emrB* and pRSFDMG_*emrA_tolC* with the known substrate CCCP [10] (Figure S3).

The EmrB-mRFP1-His-tag fluorescent fusion protein was visible as a single prominent fluorescent band via in gel fluorescence. However, on immunoblot probed for His-tag, an additional band with an electrophoretic mobility about 10 kDa above the fluorescent signal was observed (Figure 1A). A similar result was obtained for the EmrA-sfGFP-Myc-tag with a single fluorescent band in the SDS-polyacrylamide gel and an additional band visible with an electrophoretic mobility at about 15 kDa above the fluorescent species when probed with an anti-c-Myc-tag antibody (Figure 1B). The presence of these additional, non-

fluorescent species can be attributed to misfolded fusion proteins as has been previously well-documented for other membrane fluorescent protein-fusions [38–41]. The expression of TolC-Strep-tagII revealed by Western blot yielded a clear single species (Figure 1C). In sum, these results indicate that the three proteins of the complex were well-expressed in *E. coli* C41(DE3) Δ*acrAB.*

Large scale production and purification of EmrB and EmrAB-TolC complex.

EmrB has been suggested to be present in a dimeric state, on basis of EM-analysis of detergent-solubilized dimeric EmrAB particles [20]. To address the oligomeric state of EmrB in the absence of EmrA, we expressed EmrB-mRFP1 in *E. coli* C41(DE3)Δ*acrAB* harbouring p7XC3RH_*emrB* and purified it via Ni-NTA affinity chromatography. SDS-PAGE analysis indicated that EmrB-mRFP1 has an apparent molecular weight of 60 kDa (Figure 2A, B). After removal of mRFP1-His by protease 3C cleavage, EmrB displayed an electrophoretic mobility at about 40 kDa, which is less than its calculated molecular weight from the primary sequence (55.6 kDa), but in line with the aberrant behaviour of membrane proteins subjected to SDS-PAGE analysis and in particular as observed for EmrB in previous work [20]. After Apol reconstitution and subsequent size-exclusion chromatography, EmrB was recovered in the B3 and B4 fractions as shown by SDS-PAGE analysis (Figure 2C, D). The identity of EmrB was confirmed by mass spectrometry (Figure S4).

EM observations of pooled B3 and B4 fractions showed isolated particles homogeneous in size (Figure 3A). Class averages from single-particle image analysis revealed two basic forms: a 12 x 12 nm square-shaped structure with densities delineating an apparent central hole and a 12 x 17nm rectangular-shaped structure with densities delimiting an elongated hole (Figure 3B,C). Additional particles exhibiting a small string of 5 nm densities were observed and shared similar features with Apol particles (Figure 3D-F). Since EmrB

amino acid sequence predicted a small hydrophilic part protruding from the lipid membrane, densities depicting the two typical structures likely corresponded mainly to Apol densities surrounding EmrB molecules. The size of these Apol densities forming a belt around EmrB molecules suggests that the square structure likely contained one EmrB molecule while the rectangular structure which is a few nanometer longer may comprise two EmrB molecules.

Since the EmrAB-TolC complex spans two lipid membranes, the purification procedure for the intact complex for structural studies is challenging. Conventional mechanical cell disruption normally used for membrane isolation was considered less-well suited for the preservation of the entire non-covalent, native assembly. Therefore, a mild chemical lysis of cells with lysozyme and detergent was used to extract the complex. Subsequently, Ni-NTA affinity chromatography followed by size-exclusion chromatography was performed for complex enrichment (Figure 4A). SDS-PAGE analysis of the fractions indicated that fractions 22 to 26 comprised all three protein partners, whereas the next fractions were mainly containing EmrA and EmrB (Figure 4B). Fractions 22 to 26 were pooled and subjected to detergent exchange with Apol and an additional size-exclusion chromatography step (Figure 4C). The tripartite complex was mainly recovered in the A10, A11 and A12 fractions (Figure 4D) and used for further EM analysis.

Structural analysis of EmrAB-TolC complex.

Negative staining EM analysis of the combined A10, A11 and A12 fractions (see Figure 4) from the size-exclusion chromatography after reconstitution in Apol revealed elongated structures viewed from their sides (Figure 5A). An average image revealed the structure of the EmrAB-TolC complex of about 33 nm in length with an Apol belt at both extremities (Figure 5B). The length is similar to that of AcrAB-TolC efflux system structure (Figure 5C) determined under similar EM conditions [33]. The two average images revealed similar features at one side corresponding to the densities of TolC, comprising a β-barrel

channel (inside the Apol belt) and a periplasmic α-helical barrel. In contrast to the AcrAB-TolC structure, the other side corresponding to EmrA in contact with EmrB exhibit one layer of densities close to the inner membrane. TolC and EmrA appear to form a continuous channel open from the periplasmic side of the inner membrane to the outer membrane. Unlike AcrB, EmrB is predicted to not contain any substantial periplasmic domain(s), and the densities in between the lower end of TolC and the second Apol belt are 15 nm in length and most likely corresponded to EmrA including the α-helical coiled-coil and the lipoyl and β-barrel domains. The transmembrane α-helices of EmrB and the N-terminal transmembrane α-helices of EmrA are embedded in the Apol belt and therefore not visible.

Discussion

In this study, we present a strategy for the co-expression, co-purification and structural analysis of a given intact tripartite efflux system directly from bacterial cells. We applied this strategy on the thus far little understood MFS-type tripartite efflux complex EmrAB-TolC.

An EM average image of the entire EmrAB-TolC system shows an elongated structure of about 33 nm (Figure 4), which has a length similar to that of AcrAB-TolC analysed under similar conditions [33] and by cryoEM [9]. Likewise, the ABC-type tripartite efflux system MacAB-TolC efflux complex exhibits similar dimensions [7]. The MFS transporter EmrB has a predicted 14 transmembrane helices embedded into the membrane. It only presents a predicted loop containing 53 amino acid residues located between TMH13 and TMH14 towards the periplasm [42], much smaller compared to the periplasmic loops present in the RND transporters (approx. 600 amino acid residues per protomer, *e.g.* trimeric AcrB, MexB)[43,44] or dimeric MacB (approx. 220 amino acid residues per protomer) [7]. Therefore, the densities observed between the periplasmic end of TolC and the second Apol belt (corresponding to the inner membrane) can be assigned to EmrA alone (Figure 5B). The

length of the periplasmic region of EmrA (about 15 nm) is shorter than the 18.5 nm length described for the EmrA homolog from *Aquifex aeolicus* (aaEmrA) [18]. Sequence alignment and structure modelling predicts that EmrA from *E coli* (ecEmrA) indeed presents an α-helical coiled-coil domain shorter than that of aaEmrA (Figure S5 and S6) [18]. Given the length of the ecEmrA, the interaction with the periplasmic α-helical barrel of TolC could possibly correspond to a 'tip-to-tip' interaction as observed for other tripartite efflux systems [7,9,45] (Figure S6). The stoichiometry of the EmrAB complex was previously analysed corresponding to a so called 'dimer-of-dimers' in a physiological state [20]. However, it is unclear how such organization could interact with a trimeric TolC. The side view of the TolC-EmrAB complex did not resemble the 'dimer-of-dimers' EmrAB complex but is in favour of a hexameric arrangement of EmrA similar to other types of adaptor proteins (e.g AcrA, MacA) in a 'tip-to-tip' contact with TolC (Figure S6). As EmrB was completely embedded in the inner Apol belt, there is no direct interaction between EmrB and TolC expected. The oligomerization state of EmrB remains speculative, however, from the dimensions of the β-barrel domain of EmrA at the inner membrane proximal side, we tentatively modelled one EmrB protomer as previous proposed model [18].

The strategy to isolate a native and intact tripartite system may be favourable for other tripartite systems. The negative staining EM data provides first new insights on the structure of the EmrAB-TolC system and was conducted without artificial covalent linking between the subunit components of the pump system as has been done for the AcrAB-TolC and MacAB-TolC structures [6,7]. The overall length of EmrAB-TolC complex is similar to that of AcrAB-TolC with a likely tip-to-tip interaction between EmrA and TolC forming an extended periplasmic canal with at least similar length as the periplasmic tunnels shown on other known tripartite complexes. Future research will be to determine the interaction sites of EmrA with EmrB. Since EmrA contains a monotopic helical anchor in the inner membrane, possible

interaction between EmrA and EmrB might be between the transmembrane regions. In addition, the small periplasmic loop predicted between TMH13 and TMH14 might be another contact region between the two components of this tripartite setup. To analyse these interactions, higher resolution Cryo-EM structures are needed.

Acknowledgments

This work has benefited from the facilities of UMS3033/US001-IECB. The authors thank Céline Gounou for technical assistance. NY is recipient of a fellowship from University of Bordeaux-IdeX international program. This work was supported by the German Research Foundation (DFG-SFB 807, Transport and Communication across Biological Membranes).

References

[1] X.-Z. Li, P. Plésiat, H. Nikaido, The challenge of efflux-mediated antibiotic resistance in Gram-negative bacteria, Clin. Microbiol. Rev. 28 (2015) 337–418. https://doi.org/10.1128/CMR.00117-14.

[2] K. Poole, Efflux-mediated antimicrobial resistance, J. Antimicrob. Chemother. 56 (2005) 20–51. https://doi.org/10.1093/jac/dki171.

[3] Y. Pu, Z. Zhao, Y. Li, J. Zou, Q. Ma, Y. Zhao, Y. Ke, Y. Zhu, H. Chen, M.A.B. Baker, H. Ge, Y. Sun, X.S. Xie, F. Bai, Enhanced Efflux Activity Facilitates Drug Tolerance in Dormant Bacterial Cells, Mol. Cell. 62 (2016) 284–294. https://doi.org/10.1016/j.molcel.2016.03.035.

[4] D. Du, X. Wang-Kan, A. Neuberger, H.W. van Veen, K.M. Pos, L.J.V. Piddock, B.F. Luisi, Multidrug efflux pumps: structure, function and regulation, Nat. Rev. Microbiol. 16 (2018) 523–539. https://doi.org/10.1038/s41579-018-0048-6.

[5] I. Jo, J.-S. Kim, Y. Xu, J. Hyun, K. Lee, N.-C. Ha, Recent paradigm shift in the assembly of bacterial tripartite efflux pumps and the type I secretion system, J. Microbiol. Seoul Korea. 57 (2019) 185–194. https://doi.org/10.1007/s12275-019-8520-1.

[6] D. Du, Z. Wang, N.R. James, J.E. Voss, E. Klimont, T. Ohene-Agyei, H. Venter, W. Chiu, B.F. Luisi, Structure of the AcrAB-TolC multidrug efflux pump, Nature. 509 (2014) 512–515. https://doi.org/10.1038/nature13205.

[7] A.W.P. Fitzpatrick, S. Llabrés, A. Neuberger, J.N. Blaza, X.-C. Bai, U. Okada, S. Murakami, H.W. van Veen, U. Zachariae, S.H.W. Scheres, B.F. Luisi, D. Du, Structure of the MacAB-TolC ABC-type tripartite multidrug efflux pump, Nat. Microbiol. 2 (2017) 17070. https://doi.org/10.1038/nmicrobiol.2017.70.

[8] X. Shi, M. Chen, Z. Yu, J.M. Bell, H. Wang, I. Forrester, H. Villarreal, J. Jakana, D. Du, B.F. Luisi, S.J. Ludtke, Z. Wang, In situ structure and assembly of the multidrug efflux pump AcrAB-TolC, Nat. Commun. 10 (2019) 2635. https://doi.org/10.1038/s41467-019-10512-6.

[9] Z. Wang, G. Fan, C.F. Hryc, J.N. Blaza, I.I. Serysheva, M.F. Schmid, W. Chiu, B.F. Luisi, D. Du, An allosteric transport mechanism for the AcrAB-TolC multidrug efflux pump, ELife. 6 (2017). https://doi.org/10.7554/eLife.24905.

[10] O. Lomovskaya, K. Lewis, Emr, an Escherichia coli locus for multidrug resistance, Proc. Natl. Acad. Sci. U. S. A. 89 (1992) 8938–8942. https://doi.org/10.1073/pnas.89.19.8938.

[11] H. Furukawa, J.T. Tsay, S. Jackowski, Y. Takamura, C.O. Rock, Thiolactomycin resistance in Escherichia coli is associated with the multidrug resistance efflux pump encoded by emrAB, J. Bacteriol. 175 (1993) 3723–3729. https://doi.org/10.1128/jb.175.12.3723-3729.1993.

[12] O. Lomovskaya, K. Lewis, A. Matin, EmrR is a negative regulator of the Escherichia coli multidrug resistance pump EmrAB, J. Bacteriol. 177 (1995) 2328–2334. https://doi.org/10.1128/jb.177.9.2328-2334.1995.

[13] F. Puértolas-Balint, O. Warsi, M. Linkevicius, P.-C. Tang, D.I. Andersson, Mutations that increase expression of the EmrAB-TolC efflux pump confer increased resistance to nitroxoline in Escherichia coli, J. Antimicrob. Chemother. (2019). https://doi.org/10.1093/jac/dkz434.

[14] J. Heng, Y. Zhao, M. Liu, Y. Liu, J. Fan, X. Wang, Y. Zhao, X.C. Zhang, Substrate-bound structure of the E. coli multidrug resistance transporter MdfA, Cell Res. 25 (2015) 1060–1073. https://doi.org/10.1038/cr.2015.94.

[15] Y. Yin, X. He, P. Szewczyk, T. Nguyen, G. Chang, Structure of the multidrug transporter EmrD from Escherichia coli, Science. 312 (2006) 741–744. https://doi.org/10.1126/science.1125629.
[16] P.W. Fowler, M. Orwick-Rydmark, S. Radestock, N. Solcan, P.M. Dijkman, J.A. Lyons, J. Kwok, M. Caffrey, A. Watts, L.R. Forrest, S. Newstead, Gating topology of the proton-coupled oligopeptide symporters, Struct. Lond. Engl. 1993. 23 (2015) 290–301. https://doi.org/10.1016/j.str.2014.12.012.
[17] E.M. Quistgaard, C. Löw, F. Guettou, P. Nordlund, Understanding transport by the major facilitator superfamily (MFS): structures pave the way, Nat. Rev. Mol. Cell Biol. 17 (2016) 123–132. https://doi.org/10.1038/nrm.2015.25.
[18] P. Hinchliffe, N.P. Greene, N.G. Paterson, A. Crow, C. Hughes, V. Koronakis, Structure of the periplasmic adaptor protein from a major facilitator superfamily (MFS) multidrug efflux pump, Febs Lett. 588 (2014) 3147–3153. https://doi.org/10.1016/j.febslet.2014.06.055.
[19] M.I. Borges-Walmsley, J. Beauchamp, S.M. Kelly, K. Jumel, D. Candlish, S.E. Harding, N.C. Price, A.R. Walmsley, Identification of oligomerization and drug-binding domains of the membrane fusion protein EmrA, J. Biol. Chem. 278 (2003) 12903–12912. https://doi.org/10.1074/jbc.M209457200.
[20] M. Tanabe, G. Szakonyi, K.A. Brown, P.J.F. Henderson, J. Nield, B. Byrne, The multidrug resistance efflux complex, EmrAB from Escherichia coli forms a dimer in vitro, Biochem. Biophys. Res. Commun. 380 (2009) 338–342. https://doi.org/10.1016/j.bbrc.2009.01.081.
[21] V. Koronakis, A. Sharff, E. Koronakis, B. Luisi, C. Hughes, Crystal structure of the bacterial membrane protein TolC central to multidrug efflux and protein export, Nature. 405 (2000) 914–919. https://doi.org/10.1038/35016007.
[22] E.R. Geertsma, R. Dutzler, A versatile and efficient high-throughput cloning tool for structural biology, Biochemistry. 50 (2011) 3272–3278. https://doi.org/10.1021/bi200178z.
[23] K.F. Wertman, A.R. Wyman, D. Botstein, Host/vector interactions which affect the viability of recombinant phage lambda clones, Gene. 49 (1986) 253–262. https://doi.org/10.1016/0378-1119(86)90286-6.
[24] J.L. Hartley, G.F. Temple, M.A. Brasch, DNA cloning using in vitro site-specific recombination, Genome Res. 10 (2000) 1788–1795. https://doi.org/10.1101/gr.143000.
[25] R.G. Taylor, D.C. Walker, R.R. McInnes, E. coli host strains significantly affect the quality of small scale plasmid DNA preparations used for sequencing, Nucleic Acids Res. 21 (1993) 1677–1678. https://doi.org/10.1093/nar/21.7.1677.
[26] N.H. Tolia, L. Joshua-Tor, Strategies for protein coexpression in Escherichia coli, Nat. Methods. 3 (2006) 55–64. https://doi.org/10.1038/nmeth0106-55.
[27] T.A. Phillips, R.A. VanBogelen, F.C. Neidhardt, lon gene product of Escherichia coli is a heat-shock protein., J. Bacteriol. 159 (1984) 283–287.
[28] F.W. Studier, B.A. Moffatt, Use of bacteriophage T7 RNA polymerase to direct selective high-level expression of cloned genes, J. Mol. Biol. 189 (1986) 113–130. https://doi.org/10.1016/0022-2836(86)90385-2.
[29] B. Miroux, J.E. Walker, Over-production of proteins in Escherichia coli: mutant hosts that allow synthesis of some membrane proteins and globular proteins at high levels, J. Mol. Biol. 260 (1996) 289–298. https://doi.org/10.1006/jmbi.1996.0399.
[30] K.A. Datsenko, B.L. Wanner, One-step inactivation of chromosomal genes in Escherichia coli K-12 using PCR products, Proc. Natl. Acad. Sci. U. S. A. 97 (2000) 6640–6645. https://doi.org/10.1073/pnas.120163297.

[31] S. Wagner, L. Baars, A.J. Ytterberg, A. Klussmeier, C.S. Wagner, O. Nord, P.-A. Nygren, K.J. van Wijk, J.-W. de Gier, Consequences of membrane protein overexpression in Escherichia coli, Mol. Cell. Proteomics MCP. 6 (2007) 1527–1550. https://doi.org/10.1074/mcp.M600431-MCP200.
[32] C. Rascle, C. Dieryckx, J.W. Dupuy, L. Muszkieta, E. Souibgui, M. Droux, C. Bruel, V. Girard, N. Poussereau, The pH regulator PacC: a host-dependent virulence factor in Botrytis cinerea, Environ. Microbiol. Rep. 10 (2018) 555–568. https://doi.org/10.1111/1758-2229.12663.
[33] L. Daury, F. Orange, J.-C. Taveau, A. Verchère, L. Monlezun, C. Gounou, R.K.R. Marreddy, M. Picard, I. Broutin, K.M. Pos, O. Lambert, Tripartite assembly of RND multidrug efflux pumps, Nat. Commun. 7 (2016) 10731. https://doi.org/10.1038/ncomms10731.
[34] G.S. Waldo, B.M. Standish, J. Berendzen, T.C. Terwilliger, Rapid protein-folding assay using green fluorescent protein, Nat. Biotechnol. 17 (1999) 691–695. https://doi.org/10.1038/10904.
[35] D.E. Drew, G. von Heijne, P. Nordlund, J.W. de Gier, Green fluorescent protein as an indicator to monitor membrane protein overexpression in Escherichia coli, FEBS Lett. 507 (2001) 220–224. https://doi.org/10.1016/s0014-5793(01)02980-5.
[36] J.M. Hsieh, G.M. Besserer, M.G. Madej, H.-Q. Bui, S. Kwon, J. Abramson, Bridging the gap: a GFP-based strategy for overexpression and purification of membrane proteins with intra and extracellular C-termini, Protein Sci. Publ. Protein Soc. 19 (2010) 868–880. https://doi.org/10.1002/pro.365.
[37] D. Drew, D.-J. Slotboom, G. Friso, T. Reda, P. Genevaux, M. Rapp, N.M. Meindl-Beinker, W. Lambert, M. Lerch, D.O. Daley, K.-J. Van Wijk, J. Hirst, E. Kunji, J.-W. De Gier, A scalable, GFP-based pipeline for membrane protein overexpression screening and purification, Protein Sci. Publ. Protein Soc. 14 (2005) 2011–2017. https://doi.org/10.1110/ps.051466205.
[38] E.R. Geertsma, M. Groeneveld, D.-J. Slotboom, B. Poolman, Quality control of overexpressed membrane proteins, Proc. Natl. Acad. Sci. U. S. A. 105 (2008) 5722–5727. https://doi.org/10.1073/pnas.0802190105.
[39] Z. Zhang, G. Kuipers, Ł. Niemiec, T. Baumgarten, D.J. Slotboom, J.-W. de Gier, A. Hjelm, High-level production of membrane proteins in E. coli BL21(DE3) by omitting the inducer IPTG, Microb. Cell Factories. 14 (2015) 142. https://doi.org/10.1186/s12934-015-0328-z.
[40] G. Kuipers, A. Karyolaimos, Z. Zhang, N. Ismail, G. Trinco, D. Vikström, D.J. Slotboom, J.-W. de Gier, The tunable pReX expression vector enables optimizing the T7-based production of membrane and secretory proteins in E. coli, Microb. Cell Factories. 16 (2017). https://doi.org/10.1186/s12934-017-0840-4.
[41] L. Wang, C. Quan, B. Liu, Y. Xu, P. Zhao, W. Xiong, S. Fan, Green fluorescent protein (GFP)-based overexpression screening and characterization of AgrC, a Receptor protein of quorum sensing in Staphylococcus aureus, Int. J. Mol. Sci. 14 (2013) 18470–18487. https://doi.org/10.3390/ijms140918470.
[42] emrB - Multidrug export protein EmrB - Escherichia coli (strain K12) - emrB gene & protein, (n.d.). https://www.uniprot.org/uniprot/P0AEJ0 (accessed January 6, 2020).
[43] S. Murakami, R. Nakashima, E. Yamashita, A. Yamaguchi, Crystal structure of bacterial multidrug efflux transporter AcrB, Nature. 419 (2002) 587–593. https://doi.org/10.1038/nature01050.
[44] G. Sennhauser, M.A. Bukowska, C. Briand, M.G. Grütter, Crystal structure of the multidrug exporter MexB from Pseudomonas aeruginosa, J. Mol. Biol. 389 (2009) 134–145. https://doi.org/10.1016/j.jmb.2009.04.001.

[45] K. Tsutsumi, R. Yonehara, E. Ishizaka-Ikeda, N. Miyazaki, S. Maeda, K. Iwasaki, A. Nakagawa, E. Yamashita, Structures of the wild-type MexAB–OprM tripartite pump reveal its complex formation and drug efflux mechanism, Nat. Commun. 10 (2019) 1520. https://doi.org/10.1038/s41467-019-09463-9.

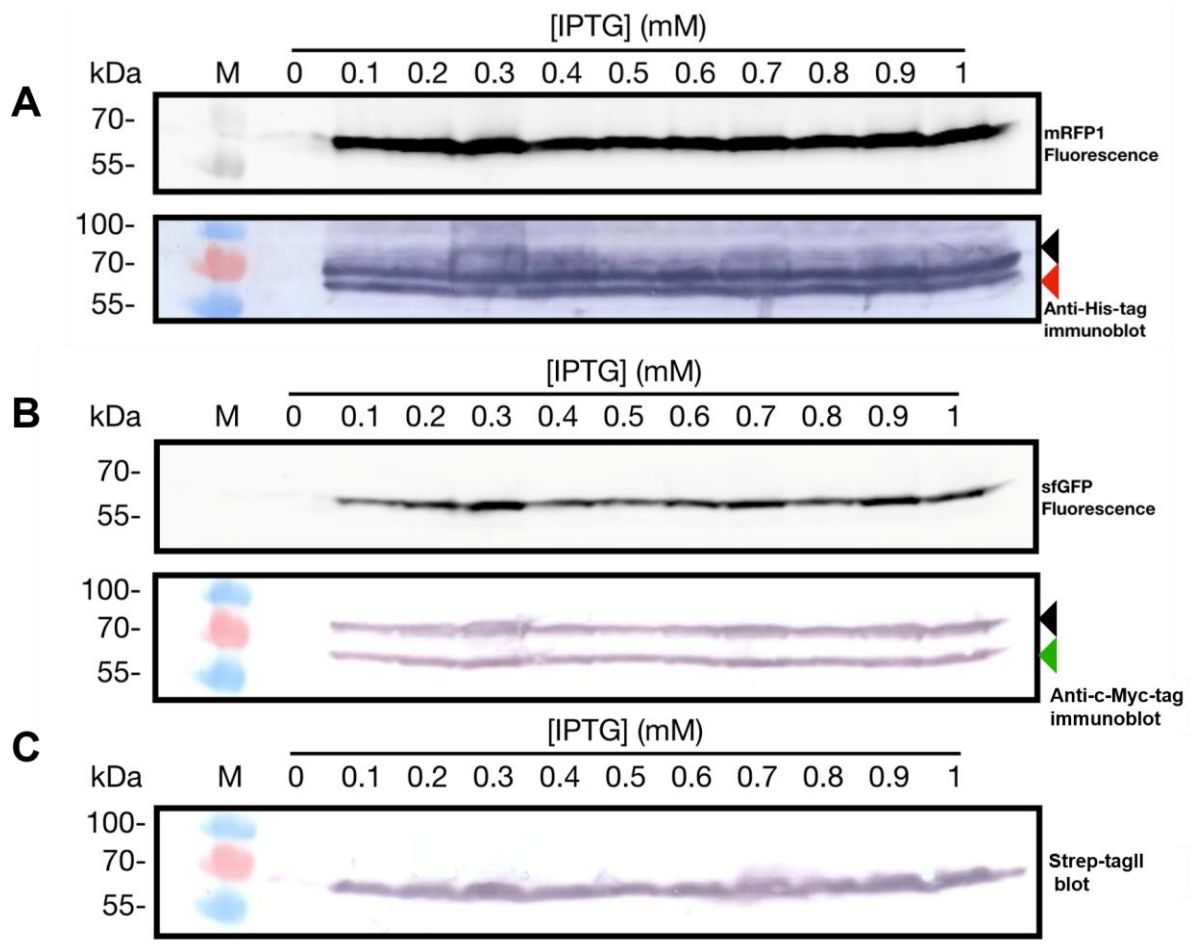

Figure 1. In gel fluorescence SDS-PAGE and Western blot analysis of EmrB-mRFP1-His EmrA-sfGFP-myc and TolC-Strep-tagII fusion proteins. All fusion proteins were expressed simultaneously in *E. coli* C41(DE3)Δ*acrAB* cells.

A) (*Upper*) *In gel* mRFP1 fluorescence used as marker for the expression of EmrB. (*Lower*) Immunoblot of the same gel to detect EmrB with anti-His antibody. B) (*Upper*) *In gel* sfGFP fluorescence used as marker for the expression of EmrA. (*Lower*) Immunoblot of the same gel to detect EmrA using anti-c-Myc antibody. C) Western blot analysis with Strep-Tactin Alkaline Phosphatase conjugate to detect TolC-Strep-tagII. Coloured and black arrows indicate the positions of fluorescent and non-fluorescent species of mRFP1 and sfGFP fusion proteins respectively. Cells were induced with different final concentrations of IPTG as described in Material and Methods. Each lane contained 15 µl of total cell extract (OD_{600} = 10).

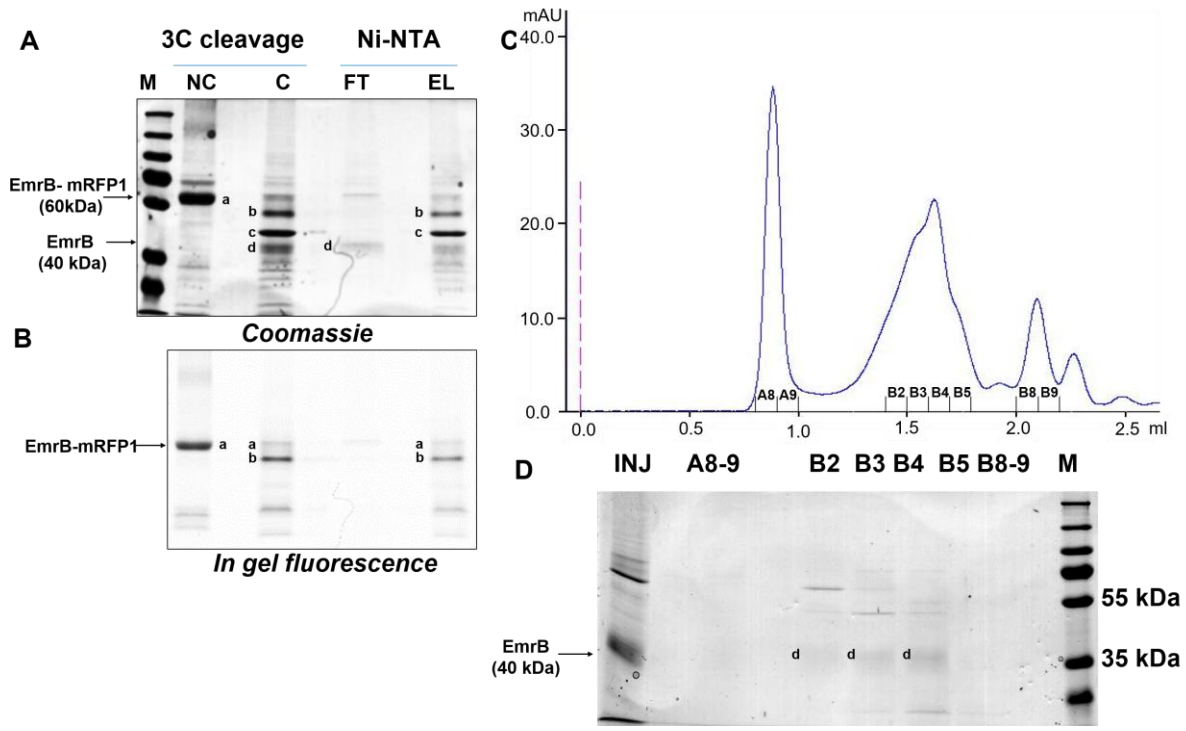

Figure 2. EmrB analysis after mRFP1-His cleavage.

A) Coomassie-Brilliant-Blue stained gel after SDS-PAGE analysis of affinity-purified EmrB-mRFP1 before (NC) and after protease 3C cleavage (C) followed by an additional reverse Ni-NTA affinity purification Bands annotated as follows: a. EmrB-mRFP-His fusion protein, b. mRFP1-His, c. Protease 3C, d. EmrB. B) In-gel mRFP1 fluorescence analysis of the same SDS-polyacrylamide gel shown in (A). The migration profile of EmrB-RFP1-His corresponds to 60 kDa and that of EmrB 40 kDa before and after 3C protease cleavage respectively. After cleavage, no fluorescence signal is recovered in flow-through (FT). C) Size-exclusion chromatography profile of EmrB after mRFP1 cleavage using Superose 6 column. 35 µg of EmrB sample were injected (dashed line). D) Coomassie Brilliant Blue-stained gel after SDS-PAGE analysis of the indicated SEC fractions. Fractions B2 to B4 contained EmrB (arrow, and annotated as d). INJ corresponds to cleaved EmrB sample stabilized with Apols. Molecular weight standards (M) correspond to the PagerulerPlus prestained protein ladder (Thermoscientific).

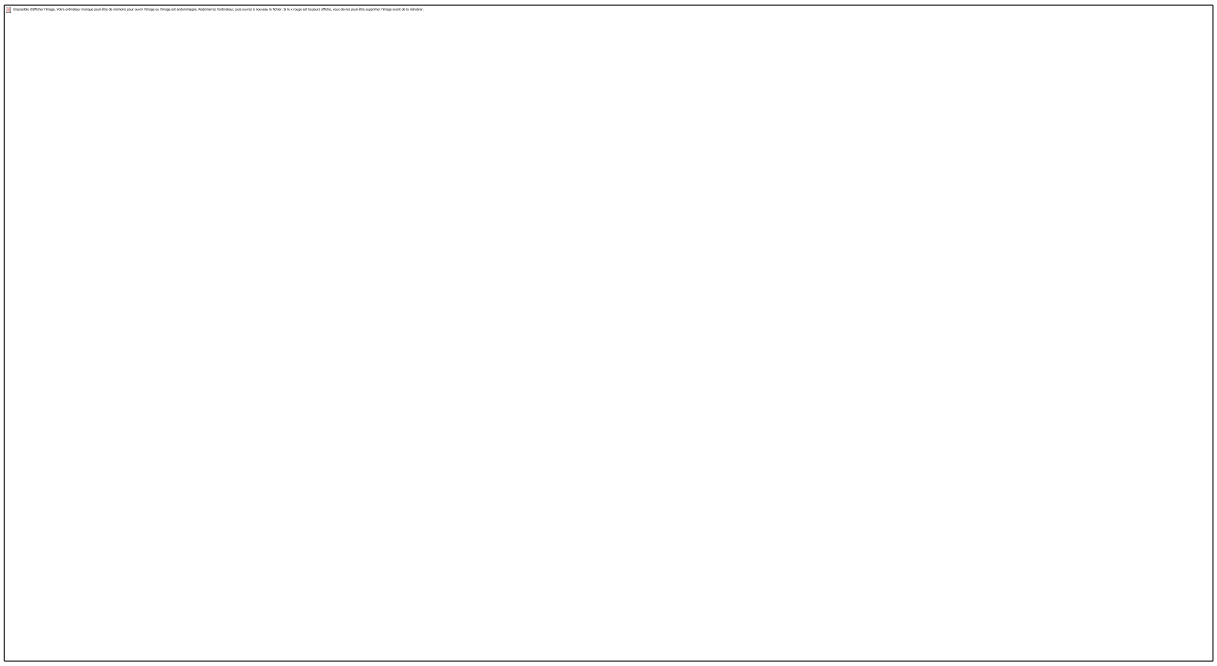

Figure 3. TEM analysis of EmrB

A) Representative negative stain image of purified EmrB reconstituted in Apol. B-D) 2D class averaging of particles showing square-shaped structures (B) and rectangular-shaped structures (C). D) Averages exhibiting small size particles resembling those in (F). E) Representative negative stain image of Apol. F) 2D class averages of particles (shown in E) display strings of small densities. Scale bars A and E:100 nm, B-D,F: 10 nm.

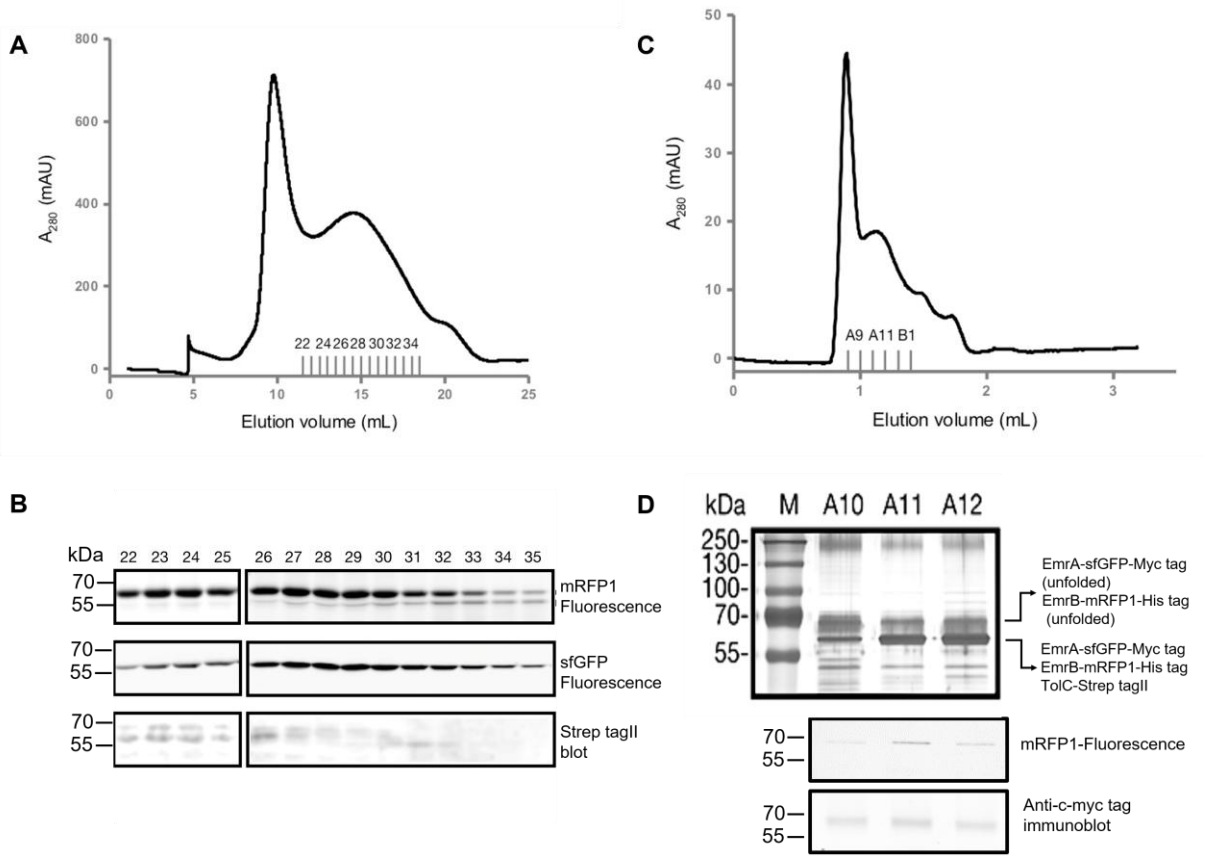

Figure 4. Large-scale co-purification analysis of EmrAB-TolC.

A) Size-exclusion chromatography profile of the co-purification sample derived from Ni-NTA chromatography in buffer containing 0.025% DDM. B) In-gel fluorescence SDS-PAGE and Western blot analysis of the indicated SEC fractions. The first peak at 10 mL elution volume corresponds to aggregates. Fractions 22 to 26 contained mainly all three protein partners. C) Size-exclusion chromatography profile of EmrAB-TolC stabilized with Apol. D) Silver-stained SDS gel of the indicated SEC fractions. The band labels corresponding to each component are indicated on the right. (Below) In gel mRFP1 fluorescence and immunoblot using anti-c-Myc antibody to detect EmrB-mRFP1-His and EmrA-sGFP-myc.

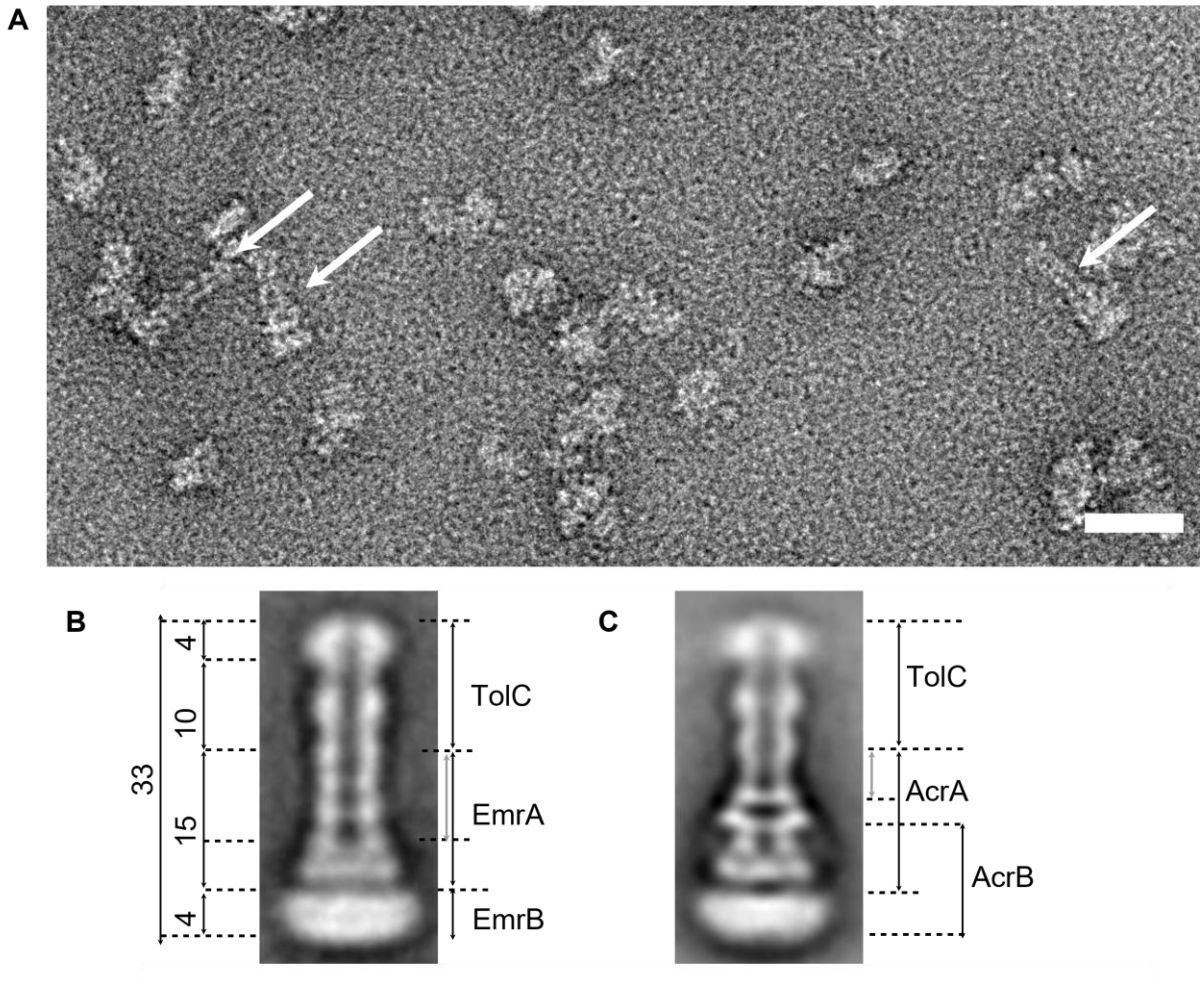

Figure 5. TEM analysis of the tripartite EmrAB-TolC efflux system.

A) Field of view showing side views of EmrAB-TolC assemblies evidenced by the white arrows (scale bar, 30 nm). B) Average image of the EmrAB-TolC complex showing densities corresponding to TolC, EmrA and Apol belts at both extremities (distances between these components are indicated in nm). C) For comparison, an average image obtained under similar EM conditions of the AcrAB-TolC complex reconstituted as published previously (Daury et al 2016). The densities corresponding to the three components are indicated. In the periplasmic part, note that the density overlap encountered for AcrA and AcrB is not predicted for EmrA and EmrB. The grey arrows indicate the α-helical coiled-coil domains of EmrA (B) or AcrA (C).

Supplementary information

Structural characterization of the EmrAB-TolC efflux complex from *E. coli*

Narek Yousefian[1,3], Alina Ornik-Cha[3], Sylvie Poussard[1#], Marion Decossas[1#], Melanie Berbon[1], Laetitia Daury[1], Jean-Christophe Taveau[1], Jean-William Dupuy[2], Selena Đorđević[3], Olivier Lambert[1 *]and Klaas M. Pos[3] *

[1]Univ. Bordeaux, CBMN UMR 5248, Bordeaux INP, F-33600 Pessac, France.
[2]Univ. Bordeaux, Plateforme Protéome, 33000, Bordeaux, France,
[3] Institute of Biochemistry, Goethe-University Frankfurt, Max-von-Laue-Str. 9, D-60438 Frankfurt am Main, Germany

# contributed equally
* Correspondence to Klaas M. Pos (pos@em.uni-frankfurt.de) or Olivier Lambert (olivier.lambert@u-bordeaux.fr)

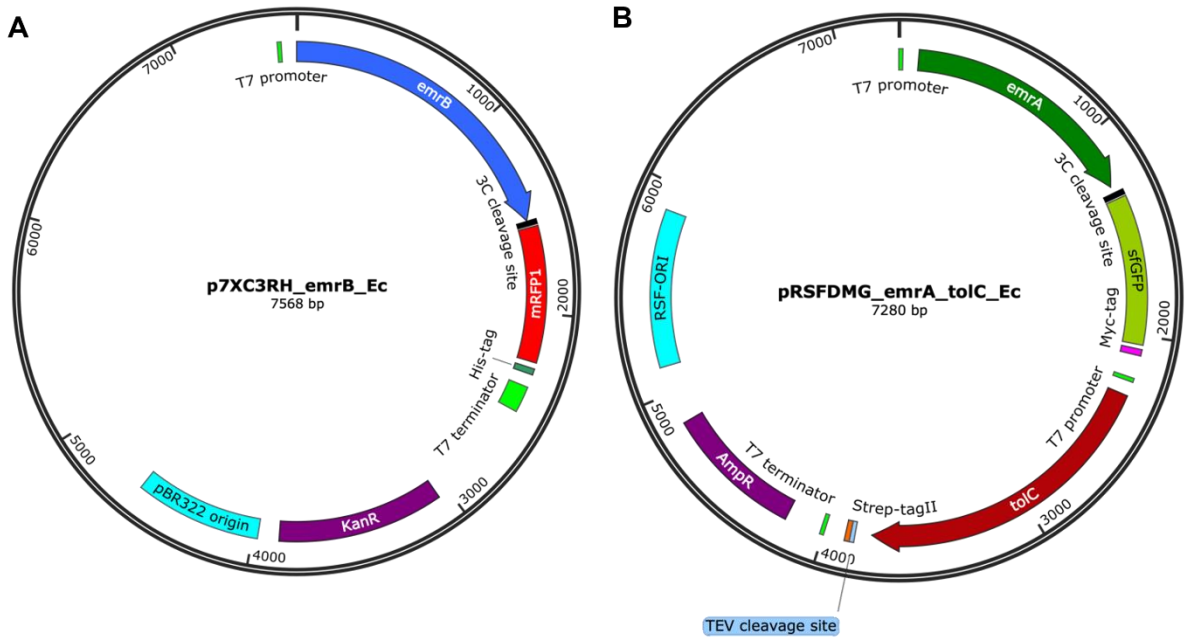

Figure S1. Schematic overview of the constructs EmrA, EmrB and TolC constructs. A) The EmrB C-terminus has been experimentally shown to be located in the cytoplasm (Daley et al., 2005). B) The periplasmic adaptor protein EmrA is linked to a Myc-tagged reporter super-folder(sf)GFP on the C-terminus. The inner membrane transporter EmrB is coupled to the His-tagged folding reporter mRFP1. For the outer membrane channel TolC, a Strep-tagII was added to the C-terminus. For every construct, the 3C cleavage site is indicated.

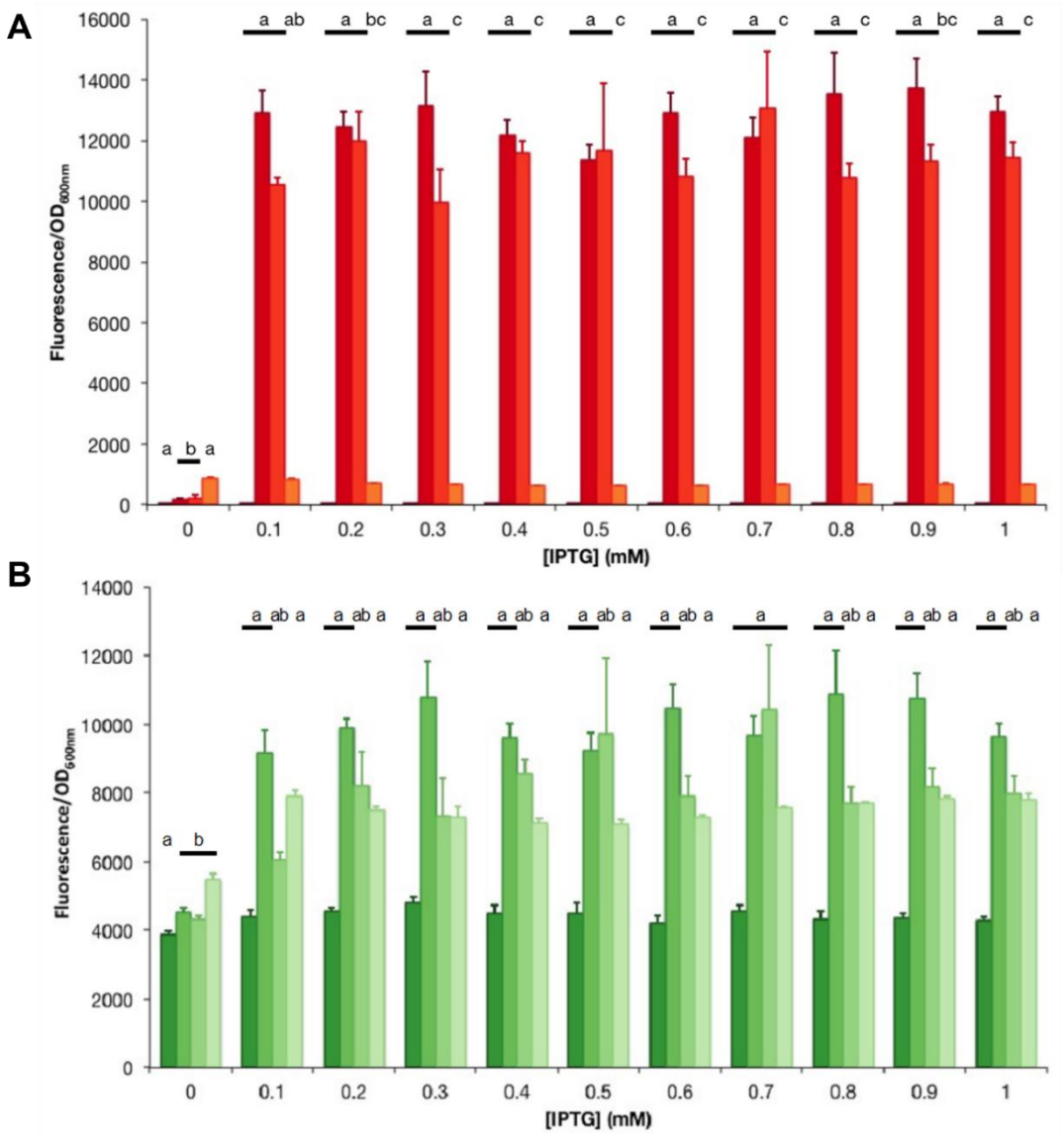

Figure S2. mRFP1- and sfGFP-based expression screen of EmrB and EmrA. (A) The overexpression of the inner membrane transporter EmrB-mRFP1 fusion was conducted in four different *E. coli* strains (BL21(DE3) -■, C41(DE3)Δ*acrAB* -■, C43(DE3) -■, BW25113(DE3)Δ*acrAB* -■) harbouring plasmid p7XC3RH_emrB_Ec. (B) The expression levels of the adaptor protein EmrA as sfGFP fusion were assayed in four different *E. coli* strains (BL21(DE3) -■, C41(DE3)Δ*acrAB* -■, C43(DE3) -■, BW25113(DE3)Δ*acrAB* -■) harbouring plasmid pRSFDMG_emrA_tolC_Ec. Variance analysis of fluorescence values for a given strain was performed using Tukey HSD test ($p<0.05$). Letters (a,b,c) and combinations of letters (ab,bc) are used to indicate differences between values according to the following rule: values sharing one letter are not significantly different.

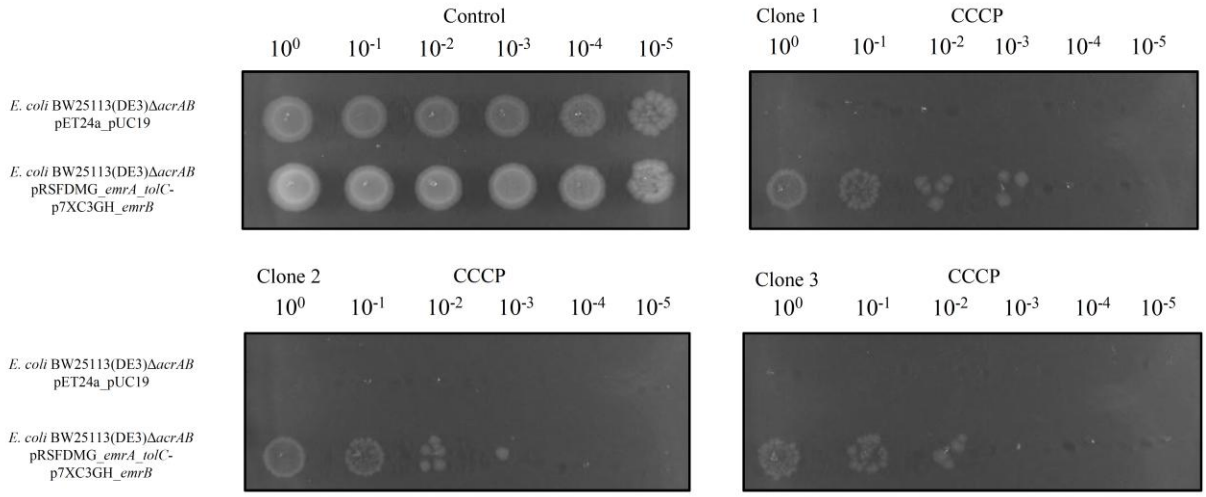

Figure S3. Drug susceptibility profile of *E. coli* BW25113(DE3) harbouring pRSFDMG_*emrA_tolC* and p7XC3GH_*emrB.* Overnight cell cultures from three colonies of *E. coli* BW25113Δ*acrAB* harbouring either pET24a and pUC19, or pRSFDMG_*emrA_tolC* and p7XC3GH_*emrB* were diluted in a series of 10-fold steps from OD_{600} 10^0 to 10^{-5} with fresh LB medium. Single droplets (4 µl) of these dilutions were spotted on Mueller-Hinton agar plates supplemented with 50 µg/ml Kanamycin, 50 µg/ml Carbenicillin, 20 µM Isopropyl-β-D-thiogalactopyranoside (IPTG) without (control) and with carbonyl cyanide m-chlorophenyl hydrazone (CCCP, 9 µg ml^{-1}). Plates were incubated overnight at 37°C. Images of the plates were produced with ImagerLAS4000. The control plate is a representative image for the control plates for all three clones.

MSQQQKPLEG AQLVIMTIAL SLATFMQVLD STIANVAIPT IAGNLGSSLS QGTWVITSFG 60
VANAISIPLT GWLAKRVGEV KLFLWSTIAF AIASWACGVS SSLNMLIFFR VIQGIVAGPL 120
IPLSQSLLLN NYPPAKRSIA LALWSMTVIV APICGPILGG YISDNYHWGW IFFINVPIGV 180
AVVLMTLQTL RGRETRTERR RIDAVGLALL VIGIGSLQIM LDRGKELDWF SSQEIIILTV 240
VAVVAICFLI VWELTDDNPI VDLSLFKSRN FTIGCLCISL AYMLYFGAIV LLPQLLQEVY 300
GYTATWAGLA SAPVGIIPVI LSPIIGRFAH KLDMRRLVTF SFIMYAVCFY WRAYTFEPGM 360
DFGASAWPQF IQGFAVACFF MPLTTITLSG LPPERLAAAS SLSNFTRTLA GSIGTSITTT 420
MWTNRESMHH AQLTESVNPF NPNAQAMYSQ LEGLGMTQQQ ASGWIAQQIT NQGLIISANE 480
IFWMSAGIFL VLLGLVWFAK PPFGAGGGGG GAHALEVLFQ 520

Figure S4. Mass spectrometry sequence coverage for EmrB. Peptides identified are shown in green highlighting. EmrB protein was identified with 30 specific and unique peptides with a coverage rate of 47.69 %.

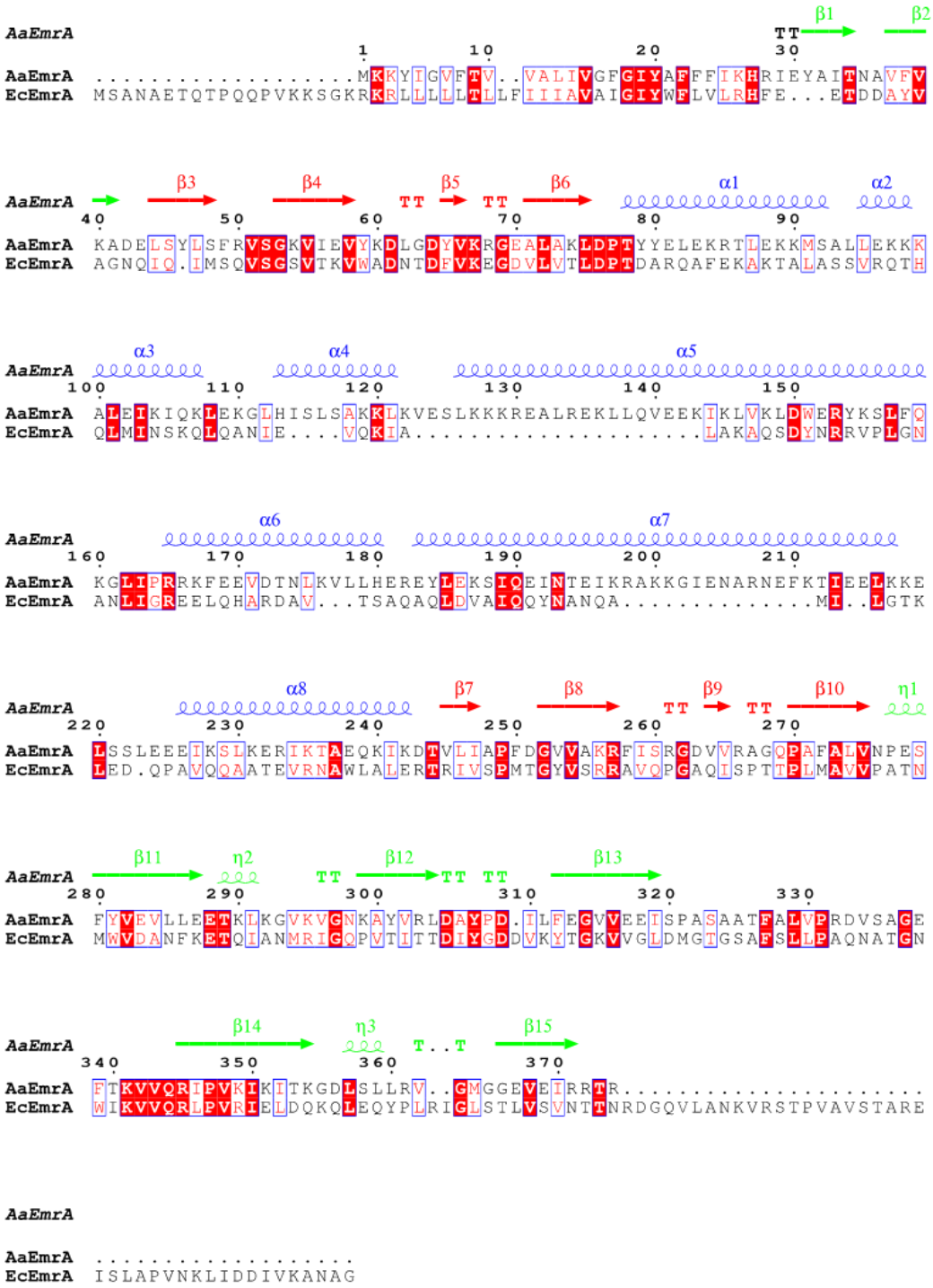

Figure S5. Sequence alignment of EmrA from *Aquifex aeolicus* (aaEmrA) and from *E coli* (ecEmrA). Identical residues are marked in white on a red background. Highly conserved residues are marked in red on a white background. Identical and conserved residues are boxed in a blue frame. The secondary structure of aaEmrA is indicated above the sequence and coloured according to the different domains (green, β-barrel; red, lipoyl; blue, α-helical coiled-coil).

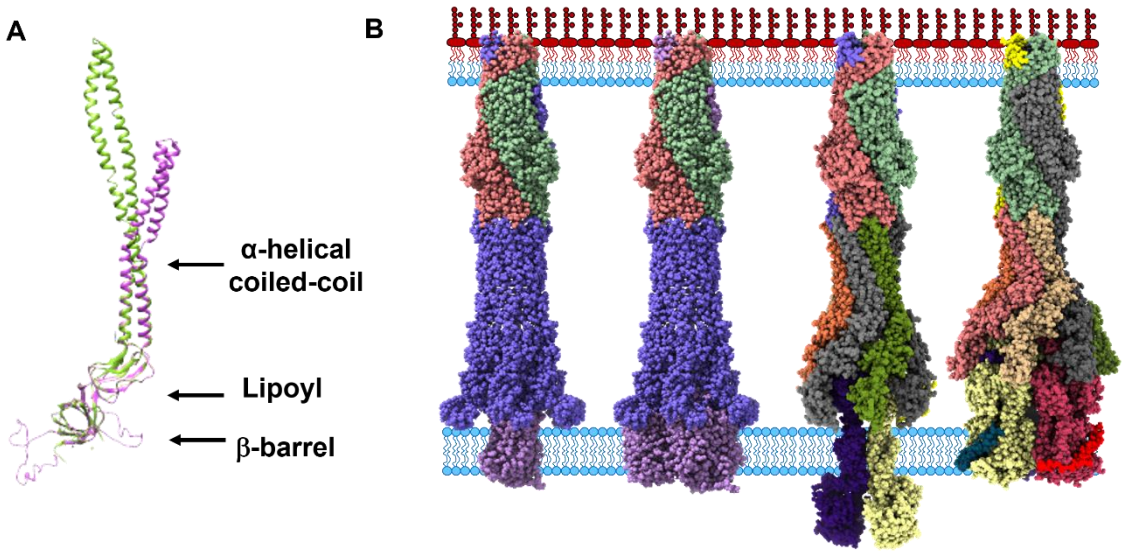

Figure S6. Overview of tripartite efflux systems from Gram-negative bacteria

A) Predicted structure of ecEmrA (purple) using the I-Tasser server (Yang et al., 2015, Roy et al., 2010; Zhang 2008) and the structure of *Aquifex aeolicus* (aaEmrA) (green) (pdb 4TKO) superimposed using Chimera. The α-helical coiled-coil of ecEmrA is shorter by 45 amino acids. The β-barrel, lipoyl and α-helical coiled-coil domains are indicated. B) Putative assembly of EmrAB-TolC (left). EmrA is shown has hexameric ring structure (blue) forming a channel through the periplasm. The six α hairpins of EmrA were modelled in a tip to tip interaction with TolC. The β-barrel and lipoyl domains are close to the inner membrane component EmrB (purple), which was modelled from its primary sequence using the Phyre2 server (Kelley et al., 2015). Since the oligomeric state of EmrB is unknown, the views of the two structures (from the left) represent monomeric or dimeric EmrB. *E. coli* MacAB-TolC (pdb 5NIK, middle right) and AcrABZ-TolC (pdb 5NG5, right) complexes are shown for comparison.

Table S1: Primers used for the insertion of the ORFs into pINITIAL

Primer name	Primer sequence 5' → 3'
EmrASapI_F	ATATATGCTCTTCTAGTAGCGCAAATGCGGAGACTCA
EmrASapI_R	TATATAGCTCTTCATGCGCCAGCGTTAGCTTTTACGA
EmrBSapI_F	ATATATGCTCTTCTAGTCAACAGCAAAAACCGCTGGA
EmrBSapI_R	TATATAGCTCTTCATGCGTGCGCACCGCCTCCGCCGC
TolCSapI_F	ATATATGCTCTTCTAGTAAGAAATTGCTCCCCATTCT
TolCSapI_R	TATATAGCTCTTCATGCGTTACGGAAAGGGTTATGAC

References

Daley DO, Rapp M, Granseth E, Melén K, Drew D, von Heijne G. Global topology analysis of the Escherichia coli inner membrane proteome. Science. 308, 1321-1323 (2005)

Kelley, L., Mezulis, S., Yates, C. *et al.* The Phyre2 web portal for protein modeling, prediction and analysis. Nature Protocols, 10, 845–858 (2015)

Roy A, Kucukural A, Zhang Y. I-TASSER: a unified platform for automated protein structure and function prediction. Nature Protocols, 5: 725-738 (2010)

Yang J, Yan R, Roy A, Xu D, Poisson J, Y Zhang Y. The I-TASSER Suite: Protein structure and function prediction. Nature Methods, 12: 7-8 (2015).

Zhang Y. I-TASSER server for protein 3D structure prediction. BMC Bioinformatics, 9, 40 (2008).